Journal of Energy Storage 18 (2018) 160–170

Contents lists available at ScienceDirect

Journal of Energy Storage

journal homepage: www.elsevier.com/locate/est

Humidity dependence of transport properties of composite materials used for thermochemical heat storage and thermal transformer appliances

Pierre D'Ans[a,*,1], Oleksandr Skrylnyk[b], Wolfgang Hohenauer[c], Emilie Courbon[b], Loïc Malet[a], Marc Degrez[a], Gilbert Descy[d], Marc Frère[b]

[a] Université libre de Bruxelles (ULB), 4MAT Department, 50 Avenue F.D. Roosevelt, CP194/03, 1050 Brussels, Belgium
[b] UMONS, Institut de Recherche en Energie – Laboratoire de Thermodynamique, 31 Boulevard Dolez, 7000 Mons, Belgium
[c] Austrian Institute of Technology GmbH (AIT), Giefinggasse 2, 1210 Vienna, Austria
[d] BE-SOL R&D, 2 rue de la Griotte, 5580 Rochefort, Belgium

ARTICLE INFO

Keywords:
Composite
Thermochemical heat storage
Calcium chloride
Mesoporous silica
Thermal conductivity
Water diffusivity

ABSTRACT

Water sorption thermochemical heat storage is a promising way to provide dwellings with renewable central heating. It requires the use of several cubic meters of materials per dwelling. Depending on the design of the heating system, specific heat and mass transfer issues occur. For instance, the heat transfer rate in reactive medium and the kinetics of sorption process determine the system thermal power. In addition, the moisture propagation during inter-seasonal storage must be understood. In this paper, the influence of the water mass uptake on the apparent thermal conductivity and apparent mass diffusivity of solid material were studied. The studied material was a composite of calcium chloride ($CaCl_2$) encapsulated in mesoporous silica with a salt content of 40–43 wt.%. The thermal conductivity was measured by the transient hot bridge method and varied from 0.13 to 0.16 $W\,m^{-1}\,K^{-1}$, having a threshold at 0.14 g/g of water mass uptake. The apparent water mass diffusivity was studied using a diffusion column. The water diffusivity – concentration dependency was established by using the modified Hall method. The apparent diffusion coefficient ranged from 3×10^{-10} to $2 \times 10^{-8}\,m^2\,s^{-1}$ in experimental conditions.

1. Introduction

Over the last twenty years, the research on thermochemical materials presented an important interest for thermal energy storage and heat transforming processes used by applications such as (i) residential heating and (ii) industrial waste heat recovery/heat upgrade. These applications aim at mitigating not only the environmental impact of the energy feedstock, but also the energy cost and efficiency of advanced economies. The design and integration of thermochemical appliances to the building sector strictly require their compactness. The size restriction condition is crucial which implies boosting the energy storage density (kW h stored per m^3) of the thermochemical storage material, as well as its specific thermal power (W per m^3). These parameters depend on the involved type of chemical bonds and kinetic characteristics.

Regarding the energy storage density, the best candidates can be found among salt hydrates. Some studies dealt with water sorption in saline conditions, where the enthalpy of dissolution is used to generate the heat [1,2]. Other works dealt with salts in solid form, like $SrBr_2$ [3–5], $MgSO_4$ [6] and $CaCl_2$ [7]. In this case, the formation of the various hydrates in the presence of water vapor results in the heat release, which can be used for the heat storage purposes:

$$MX.nH_2O(s) + mH_2O(g) \rightleftarrows MX.(m+n)H_2O(s) + \Delta H^r.$$

Where MX signifies salt; m and n are integer numbers and ΔH^r is the reaction enthalpy. This process refers to the thermal energy storage and heat transforming by the mean of solid-gas thermochemical reversible reactions. It can be extended to other sorbents like alcohols or ammonia [8,9].

The specific thermal power depends on heat and mass transfer parameters.

The mass transfer parameters are directly affected for salts hydrates by the following phenomena:

(i) Due to the crystallization of the various hydrates, the salt morphology is altered at each cycle, reducing their reversibility properties, causing the reduction of the heat amount that can be stored/

* Corresponding author.
E-mail address: pdans@ulb.ac.be (P. D'Ans).
[1] Partly detached at UMONS.

https://doi.org/10.1016/j.est.2018.04.027
Received 31 January 2018; Received in revised form 25 April 2018; Accepted 26 April 2018

released under real operating conditions [7].

(ii) Many metal halides, e.g. $CaCl_2$, LiCl, $MgCl_2$, $ZnCl_2$ etc., are very soluble in water and are even able to dissolve in their own water of crystallization: this phenomenon is known as deliquescence [7,10–12]. This leads to the salt particles agglomeration into hard blocks during the dehydration process, which limits the exchange of water molecules.

An efficient way to overcome the mentioned drawbacks is to synthesize composite materials by incorporating the hygroscopic salt into a porous solid matrix that durably maintains microscopic pathways for the water vapor penetration or release. Molecular sieves such as zeolites [13,14], metal-organic frameworks [15], carbonaceous supports such as activated carbon [16] or expanded graphite [3], as well as siliceous supports (including mesoporous silica gel) [17,18] and carbon nanotubes [8,9,19,20], have been proposed as matrices for the composite materials synthesis. Generally, the porous matrix marginally participates to the sorption process, which is mainly due to the hydration/dehydration reactions of the salt. However, the thermodynamic properties of the encapsulated salt are different from those of the bulk salt. The early proposed composite material was synthesized by Aristov et al. using $CaCl_2$ trapped in silica gel [17].

The heat transfer parameters can be somewhat improved as well to boost the specific power at the macro-scale, by the use of highly heat conductive additives with the material [3,21]. For instance, the thermal conductivity of silica gel was increased from 0.106 $W\,m^{-1}\,K^{-1}$ to 0.363 $W\,m^{-1}\,K^{-1}$ by adding aluminium scraps [21]. However, this way results in the drop of the material energy storage density, because the heat conductive additive is inert.

These considerations apply to a wide range of thermochemical energy storage systems and thermal transformer appliances designed to work with solid sorbents and water vapor under atmospheric pressure or even below, as shown on Fig. 1. The heat and mass transport properties have to be maximized for reactors shown on Fig. 1a and b. The optimization of the volume for the configuration from Fig. 1c implies the coexistence of reacted (hydrated) and unreacted (dehydrated) material fractions in a stratified storage tank. This case corresponds to a moving bed, for instance a fluidized bed. In this case, it is required that the water migration would be slow enough, so that the dehydrated material would not be contaminated by the hydrated material.

The proper design of the reactive bed (see Fig. 1a–c) by the means of computational fluid dynamics (CFD) usually requires the knowledge of parameters such as thermal conductivity, water diffusivity in the material and/or information on the bed permeability [3,4,22–29]. This issue is hard to tackle, since these values depend on several phenomena, the major of which are: real heat conduction inside the solid; free/forced convection around the shaped/powder-like material for thermal conductivity; heat and mass transport inside the single particle.

In the above-mentioned simulation works, thermal conductivity and water diffusivity values were rarely obtained from direct measurements. The CFD methods used also a set of mathematical correlations for these parameters that must be first obtained using laboratory experimental methods.

Regarding thermal conductivity, devices that expose a sample to a local heating (plate or wire) and monitor thermal transients were used or developed, to get thermal conductivity and/or diffusivity ([30], "transient hot strip": [31], "hot wire": [32,33]). Such methods have already been tested in the case of salts for thermochemical storage [34] and phase change materials [35], with a moisture controlled atmosphere in the latter case. Benchmarks have been taken for composites of the same family in [32,36] and for pure silica. It has to be noted that it is appropriate to account for the thermal conductivity of the different phases, like in [22], where distinct values were taken for $MgSO_4$ and $MgSO_4.7H_2O$. The same authors used a simple mixing rule between the solid and the gas [22]. In the work of Gaieni et al. [28], the Zehner-Schlunder relationship was used for the effective thermal conductivity [37], while Mette et al. [26] used the Winterberg relationships for thermal conductivity [38]. A review of correlations for the thermal conductivity of packed beds is given in [37].

Nevertheless, these works were related to a simple solid sorbent, being in contact with water vapor, and not to a composite material, for which the heat and mass transfer phenomena are more complex to tackle. Indeed, the heat and mass transfer rates are expected to depend on the way the salt crystals are being integrated to the supporting porous matrix, in addition to the above-mentioned phenomena. The PROMES group proposed and applied a framework based on a salt-in-matrix composite, when the matrix is much more heat conductive than the salt. By analogy with mass transfer, they introduced the concept of thermal tortuosity, to account for the more complex heat flow pathway. It was applied to $MnCl_2$ incorporated in a carbon matrix [3,16].

On the account of water diffusivity, it can be measured using water concentration profiles in a fixed packed-bed filled by the composite material and applying the Hall method. The latter is specifically suited for the concentration dependent diffusivity [39]. The obtained results can be used for water vapor migration modelling, based on the correlations like the Chen-Otmer equation mentioned in [27], but it does not apply directly to biphasic solids like in the present work. A review of existing correlations, that are applied typically to cylindrical packed bed, is available in [40], with a distinction between the transversal and longitudinal dispersion coefficients, and the influence of parameters like the particles diameter and the fluid velocity.

This work focusses on the macroscopic transport properties investigation of a novel composite material using $CaCl_2$ encapsulated into mesoporous silica gel. The pure salt is able to store 516 $kW\,h\,m^{-3}$ of hexahydrate of $CaCl_2$, considering the gain/loss of 5 mol of water per mole of $CaCl_2$. It is non toxic and particularly cheap. An improved composite was proposed based on silica gel and 43 wt.% of $CaCl_2$: a high energy storage density of 211 $kW\,h\,m^{-3}$ (upgradable) was found

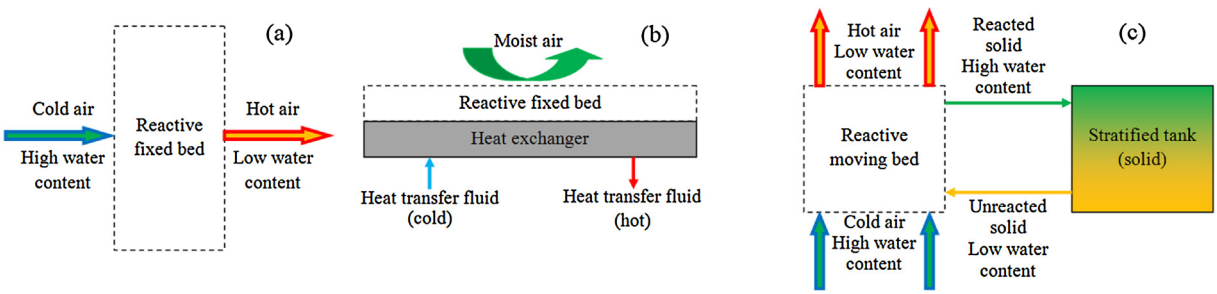

Fig. 1. Thermochemical processes and apparatus concerned by the present work. The process is shown during heat production: a) Fixed packed-bed reactor; b) Reactor (adsorber) with heat exchanging surface coated by the material (sorbent); c) Moving bed reactor with separate material (sorbent) storage.

(considering the adsorption temperature at 30 °C, the desorption temperature at 80 °C and the water vapor pressure at 1.250 kPa), with excellent reversibility. Special care was dedicated to the distribution of the salt inside the pores to avoid salt losses in open reactors. The salt was solely located inside the pores, with no excessive concentration in the outer regions of the particles [18,41].

The aim of this work is thus to measure the apparent values of thermal conductivity and water diffusivity of this composite material in stagnant conditions. Such experimental data are a prerequisite for the complete modeling and design for any of the thermochemical apparatus shown on Fig. 1. It is expected that the hydration state of the composite material influences these properties. The initial research question is thus to measure the transport properties and to study this suspected moisture influence. The experimental protocols were adapted to measure water diffusivity and thermal conductivity as a function of water concentration in the composite.

The work is organized as follows. The characterizations of the material samples manufactured under laboratory and large-scale impregnation conditions are presented in the first part of the work. Then, the transient hot bridge method (THB) was used to measure the thermal conductivity of samples under controlled atmosphere conditions. Finally, experiences on a diffusion column are presented for the mass transfer parameters and a modified Hall method was used to interpret the results. The comparison was made with a similar material synthesized by Aristov et al. [42].

2. Materials and methods

2.1. Synthesis of composite materials

The studied material is a so-called salt-in-matrix composite. The used salt is $CaCl_2$, provided by Solvay (Caso granules, 94% purity) and the support matrix is a mesoporous silica gel (SG Davisil®) provided by Grace. Two different SG grades (62 and a variant that we will denote by "62L") were used to produce the composite at the laboratory scale (0.5 kg) and at the large scale (140 kg). Both SG grades have the same average pore diameter (d_{av} = 15 nm), similar pore volume V_{s0} and specific surface area A_{sp}, but different particle diameters d_p. For SG62, d_p = 100–300 µm while for SG62L, d_p = 315–500 µm.

The synthesis method is a multi-step incipient wetness impregnation process. The synthesis protocol was described by Courbon et al. [18,41]. The dehydrated SG particles were impregnated with aqueous $CaCl_2$ solution, which volume was equal to the SG pore volume, and were dried. This process was sequentially repeated until the dry salt content has reached at least 40 wt.%.

2.2. Chemical and structural characterization

A part of the chemical and structural characterizations of SG62/$CaCl_2$ was already presented in [18].

The final salt content was verified by sample weighting and confirmed afterwards using X-ray fluorescence method. The porous characteristics were obtained from the nitrogen sorption isotherm measurement at −196 °C using a Belsorp max apparatus. Prior to the measurement, the samples were dried at 200 °C under vacuum for 10 h. The total pore volume was determined from the amount adsorbed at p/p_{vs} = 0.990. The specific surface area was estimated by a BET (Brunauer–Emett–Teller) treatment using the branch in the relative pressure between 0.05 and 0.3.

For the composite SG62L/$CaCl_2$ produced under large-scale conditions, it was necessary to verify that the impregnation was an in-depth process. This was done by impregnating particles inside a rigid mounting resin (ClaroCit®, Struers), by polishing the obtained sample till cross-sectional particles area, and then by depositing conductive carbon. Chemical composition was analyzed with scanning electron microscopy coupled to EDX (SEM-EDX (FEI)) at the central and outer parts of the composite particles.

The SG62L/$CaCl_2$ composite microstructure was studied using transmission electron microscopy (TEM) method. A thin foil of material was first extracted using focused ion beam (FIB) technique. This preparation step was made in the SEM, from a particle cross section. A selected cross section area was etched layer by layer using accelerated Ga^+ ions (30 kV, 5 nA), until a foil with a length of ~20 µm was delimited. Then, the foil was welded to a stick using carbon deposition technique and completely separated from the initial particle. It was mounted on a copper grid and then exposed to Ga^+ beam with low current to reduce the material degradation rate. Once the thickness < 100 nm was obtained, the grid was transferred to the TEM (Philips CM20® with EDX). The transfer was done rapidly, so as to avoid any degradation of the foil.

2.3. Water sorption equilibrium

The influence of the up-scaling of the synthesis protocol and the SG grade on the hydration/dehydration thermodynamic properties of composites was studied by comparing water sorption data.

Water sorption equilibrium was measured using the dynamic sorption apparatus IGASorp from Hiden Isochema. The measurements were done at 30 °C with N_2 as inert carrier gas. The humid N_2 flow rate was 250 mL min^{-1}. Prior to any sorption measurement, each sample was dried at 200 °C for 10 h by blowing the dry N_2 with 250 mL min^{-1} flow rate (heating rate: 1 °C min^{-1}). The measurements were done for relative humidity (RH) ranging from 0 to 50% RH with a step of 5% RH.

2.4. Conductivity measurements

The transient hot bridge method (THB) was used for the thermal conductivity measurements. Under ideal measurement conditions, the THB sensor is enclosed between two blocks of solid, or submerged in liquid. Thereby sufficient thermal contact between the sensor and the measured material is realized. The sensor operates in two manners: it acts (i) as a heat source that generates a constant heat flow, and (ii) as a detector of the thermal response of the material. Thus the thermal conductivity of the sample can be examined using the sensor thermal response and by solving the heat balance equation for the thermal conductivity [43–45].

Measurements of thermal conductivity were made either after the complete dehydration in a laboratory oven, or *in-situ* inside a climate chamber, on a sample exposed to the reference conditions of temperature T_a and water vapor partial pressure p_v. For this purpose, VTRK 300 climate chamber (Heraeus Vötsch) was used. It was tuned to create conditions of 10 °C < T < 90 °C for the temperature and $0.1 \leq \frac{p_v}{p_{vs}} \leq 0.9$ for the water partial pressure (p_{vs}: saturation pressure of water). A balance was used for the in-situ water uptake measurement. The schematics of the laboratory set-up are shown on Fig. 2.

The partial water vapor pressure p_v and temperature T_a program is shown on Fig. 3. The sample was first hydrated at p_v = 1.250 kPa and T_a = 35 °C, where $CaCl_2$ is expected to be in aqueous solution inside the pores. This p_v value corresponds to p_{vs} at 10 °C. In real winter conditions, it is indeed necessary to work under such a vapor pressure using 10 °C as a water vaporization temperature, attainable by an available (cheap and free) ultra-low grade heat source. Thermal conductivity was measured a first time, then temperature was progressively increased in 4 steps (50, 60, 70 and 80 °C), so as to dehydrate the composite. Each time, mass and conductivity were monitored, and the next step was started only if they have reached their new equilibrium value. The same program was then performed at p_v = 1.704 kPa.

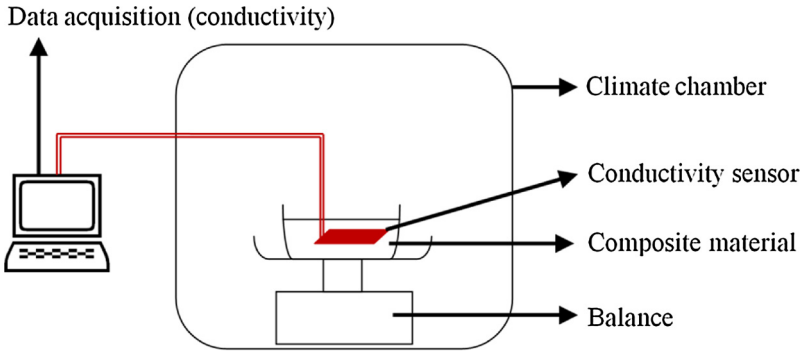

Fig. 2. Laboratory set-up for the in-situ heat conductivity measurements.

2.5. Water migration

The water migration was investigated as a function of the moisture propagation time from hydrated to dehydrated composite with a specially designed cylindrical glass column (see Fig. 4). The column diameter is 0.08 m and its height is 0.4 m. Such a geometrical aspect ratio was selected to represent the real material storage tank (see Fig. 1c). It is equipped with 10 lateral apertures of 8 mm diameter for samples extraction and analysis purposes.

The hydrated quantity of composite was prepared in VTRK300 climate chamber at T_a = 30 °C and 1.250 kPa. The dehydrated quantity of material was prepared in the laboratory oven at 150 °C. The dehydrated sample was then cooled down to 25 °C in a dry hermetic vessel. The volume ratio of hydrated and dehydrated material fractions were 1:1 of the total column volume (~2 L). Then the hydrated and dehydrated samples were introduced to the column at the initial time step and layered inside the column to form a flat interface between both material fractions.

Around 100–150 mg samples were extracted practically simultaneously from all lateral apertures, after variable time intervals, in order to measure their water concentration using the gravimetric analyzer Sartorius MA35. The extracted samples were heated up for 10 min at 150 °C and then the mass difference between before and after heating was calculated, assuming that the whole moisture content has been removed.

Concentration-distance plots were drawn at each time and the diffusion coefficient was evaluated as a function of concentration using the Hall method [39,46]. Moreover, a modified Hall method was developed in order to interprete the results (see Appendix A).

3. Results and discussion

3.1. Material characterization

The composite SG62/$CaCl_2$ has already been extensively characterized in [18]. The synthesis process was able to produce particles with homogeneous in-depth composition of 40–43 wt.% salt content. The heat storage performance was directly linked to the salt content. The water sorption process involved hydration/dehydration reactions of various hydrates of $CaCl_2$, dissolution of $CaCl_2$ tetrahydrate in the pores of the silica gel and absorption by the salt solution inside the pores of the matrix.

Since the composite SG62L/$CaCl_2$ has been synthesized under large-scale conditions and has bigger particles size than the composite SG62/$CaCl_2$ (see Table 1), it should be verified that the up-scaled manufacturing process did not affect the composite structural properties and that the salt is present throughout the particle full depth. The main structural features of SG62, SG62L and the obtained composites are summarized in Table 1.

The salt content measurement in two domains of the particles cross section area impregnated inside the resin was repeated 20 times, on 12 particles. The perimeter of measurement and typical EDX spectra are given in Fig. 5a. A rectangle aspect ratio was drawn as 10:1, forming a row of 10 squares. The 1st and the 5th squares were taken as the measurement areas, respectively denoted "out" and "in" on Fig. 5a. The EDX spectra were acquired on these squares and compared. The peaks of Si, Ca and Cl were similar in both cases, showing that there was no significant chemical composition difference throughout the particle. The local $CaCl_2$ content was then calculated, assuming that the matrix

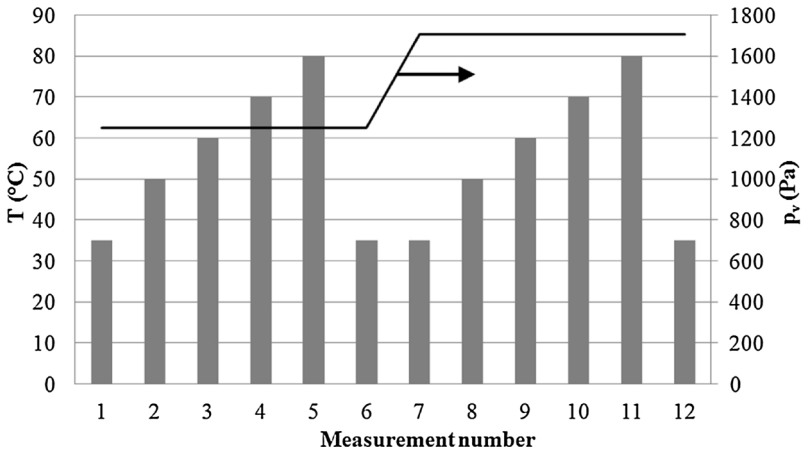

Fig. 3. Roadmap of experiments: T_a and p_v profiles used for thermal conductivity measurements.

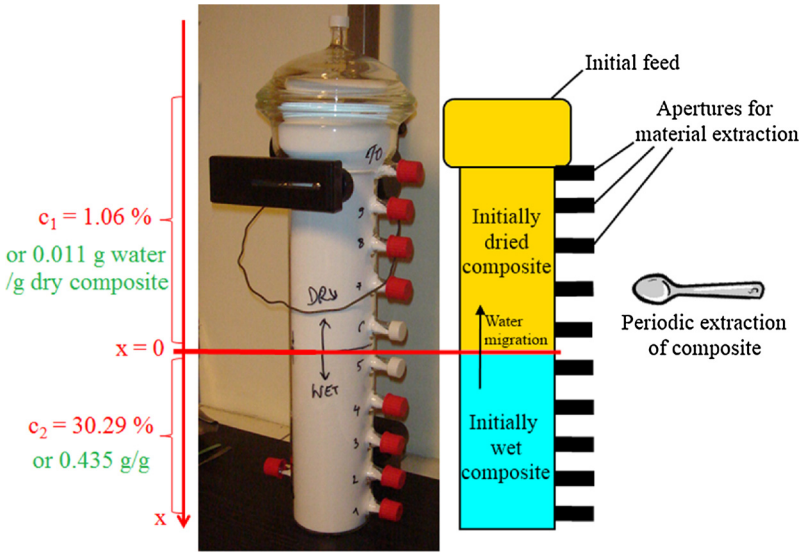

Fig. 4. Vessel used to investigate the water migration. The space coordinates for diffusion profiles are numbered. The initial water content of dehydrated material fraction is c_1 and hydrated fraction is c_2.

Table 1
Silica gel and composites characteristics. "Exp." denotes experimental data, "prod.", data from the producer.

Sample	V_{s0} ($cm^3\,g^{-1}$)	A_{sp} ($m^2\,g^{-1}$)	d_p (μm)	Production scale (kg)	Used for:
Davisil® grade 62 (SG62)	1.06 (exp.) 1.15 (prod.)	320 (exp.) 300 (prod.)	100–300 (prod.)	0.5	Thermal conductivity
SG62/$CaCl_2$ (43 wt.%)	0.38 (exp.)	75 (exp.)			
Davisil® SG62L	1.15 (prod.)	300 (prod.)	315–500 (prod.)	140	Water diffusivity
SG62L/$CaCl_2$ (40–42 wt.%)	0.30 (exp.)	129 (exp.)			

has the stoeichiometry SiO_2. The results appear in Fig. 5b. It can be seen that the central part of all the analyzed particles is rich in $CaCl_2$. Therefore, the up-scaled impregnation process was successful. Furthermore, the calculated $\frac{\left(Ca/Si\right)_{in}}{\left(Ca/Si\right)_{out}}$ ratio varies in the range between 0.72 and 1.96, or is equal in average to 1.3 ± 0.3. This indicates that there is more salt in the central part of the particle than in the outer interface area. This result also confirms the same trend observed for the composite SG62/$CaCl_2$ as described in [18]. The fact that the salt is generally concentrated in the central region of the particles is beneficial in that it helps avoiding salt losses during operations. However, there is a significant heterogeneity from particle to particle, but the average value is quite close to the XRF measurements, that range from 40 to 42 wt.%.

The material is composed of the irregularly shaped crystals with nanoscale size < 50 nm (Fig. 6). The initial SG substrate could not be distinguished from $CaCl_2$ crystals by its morphology within the intensive EDX analysis that pointed out that the salt deposition was homogeneous at the scale of < 1 μm.

3.2. Water sorption equilibrium

Water sorption equilibrium data, measured at 30 °C for hydration (denoted as "ads.") and dehydration (denoted as "des.") of SG62/$CaCl_2$ and SG62L/$CaCl_2$ composites, are shown in Fig. 7. The hysteresis region can be observed for the plots "SG62/$CaCl_2$ ads." and "SG62/$CaCl_2$ des." in the range of p_v/p_{vs} values between 0.05 and 0.15. For this composite, the plateau that corresponds to $CaCl_2$ dihydrate state also appears between 0.05 and 0.1 of p_v/p_{vs} on the plot "SG62/$CaCl_2$ ads.". On the contrary, this plateau disappears and the hysteresis is reduced for the

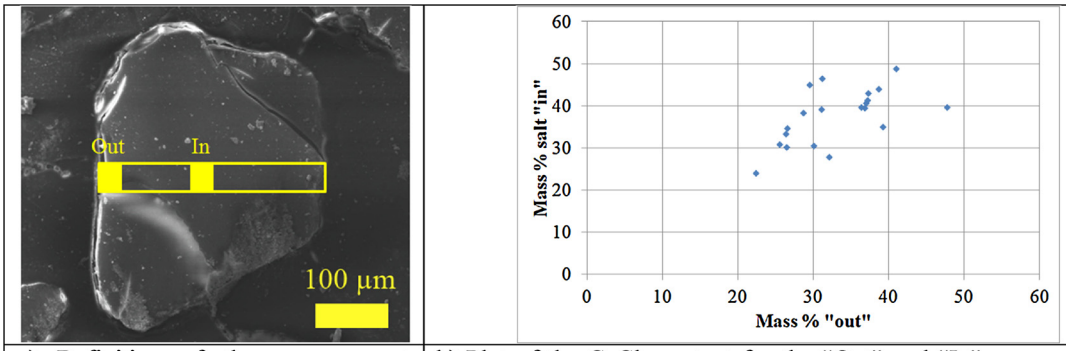

a) Definition of the measurement areas on the particle cross section.

b) Plot of the $CaCl_2$ content for the "Out" and "In" squares on 20 pairs of locations.

Fig. 5. EDX analysis results of SG62L/$CaCl_2$ composite.

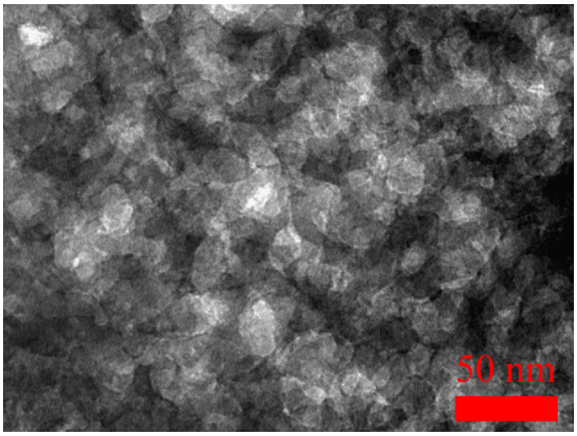

Fig. 6. TEM micrograph of SG62L/$CaCl_2$ foil.

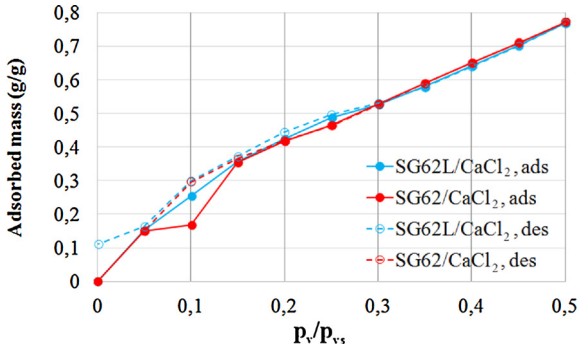

Fig. 7. Water sorption equilibrium plots of SG62/$CaCl_2$ [36] and SG62L/$CaCl_2$ composites measured at 30 °C during hydration (denoted as "ads.") and dehydration (denoted as "des.").

plots "SG62L/$CaCl_2$ ads." and "SG62L/$CaCl_2$ des.". This means that the $CaCl_2$ dihydrate exists in a smaller pressure range for the SG62L/$CaCl_2$ composite than for the SG62/$CaCl_2$. Sorption isotherm plots are identical and grow up linearly for both materials, when $p_v/p_{vs} > 0.15$. This region corresponds to the absorption of water in the salt solution trapped in the silica gel pores. For both composites, the salt appears neither in mono nor tetrahydrate states, as follows from the shape of isotherm plots (see Fig. 7). Since the water sorption properties of both composites at 30 °C are identical, these materials can be interchangeably used in the investigation of heat and mass transfer processes. The only exception is the point at $p_v/p_{vs} = 0.1$, which was excluded from the operating conditions to accomplish this study.

3.3. Thermal conductivity

At each new temperature step, thermal conductivity undergoes some variations after having reached a new steady-state. Transient values of apparent thermal conductivity are represented in Fig. 8(a, b). It can be observed that for T_a ranging between 50 and 70 °C, independently on p_v, the thermal conductivity first rapidly increases, but then decreases and reaches the steady-state. This behavior was observed at most for two days before the steady-state has been clearly reached in four days. Variations of thermal conductivity values during the transient period were $< 0.2\,W\,m^{-1}\,K^{-1}$.

It has to be noted that any thermal source must be equal to zero when calculating the thermal conductivity under isothermal conditions. Unavoidably, this condition did not hold true for the application of the THB method in the middle of the sorption process. THB results, detected during transient phase of humidification of the solid matrix, must not be interpreted as standalone thermal conductivity, but as a superposition of thermal transport and thermochemical enthalpy related effects.

Therefore minimum two phenomenological reasons can be given to explain the transient values. The first reason is that the temperature increase leads to the progressive dehydration and salt exothermal recrystallization, since the salt was in the solution state inside the silica gel pores when the composite was initially hydrated at 35 °C and $p_v > 1.250$ kPa. The second reason is that the dehydration process locally affects the water vapor partial pressure and the bed temperature.

Fig. 9a gives the steady-state values, defined as the average of 2 or more final values after at least 36 h. Error bars were obtained using a Student variable. Steady-state conductivities do not differ significantly from more than 10%. Conductivity in dry conditions is also given. The step of the thermal conductivity is observed near 60 °C, which is considered to be significant because its magnitude is bigger than the uncertainty. Under hydrated conditions conductivity is significantly higher than under dehydrated conditions. As follows from Fig. 9a, the thermal conductivity of dehydrated composite material linearly grows up from $0.125\,W\,m^{-1}\,K^{-1}$ (at room temperature) to $0.1325\,W\,m^{-1}\,K^{-1}$ (at 80 °C). This is a typical trend for insulating materials. The opposite trend is observed for the hydrated composite, for which the thermal conductivity is higher than for the dehydrated material and it diminishes as far as the temperature grows up. In the presence of water, an opposite trend is observed. Thermal conductivity is higher and decreases with temperature. The biggest gap of conductivity appears at a higher temperature at 1.704 kPa than at 1.250 kPa, because chemical equilibrium shifts towards higher water content (see Fig. 7).

For a better understanding of these effects, Fig. 9b represents the data of Fig. 9a using the aggregated function $\lambda = f(c)$ of water uptake c for x-axis. A correlation exists, allocating c to be the governing parameter, excluding temperature, with a possible threshold, as already described in [36].

The complete understanding of $\lambda = f(c)$ is obtained by analyzing the individual components of the composite, i.e. $CaCl_2$ and SG matrix.

Regarding Fig. 9, several salt states in the SG matrix have to be considered: anhydrous, hydrates and aqueous solution. Relevant data

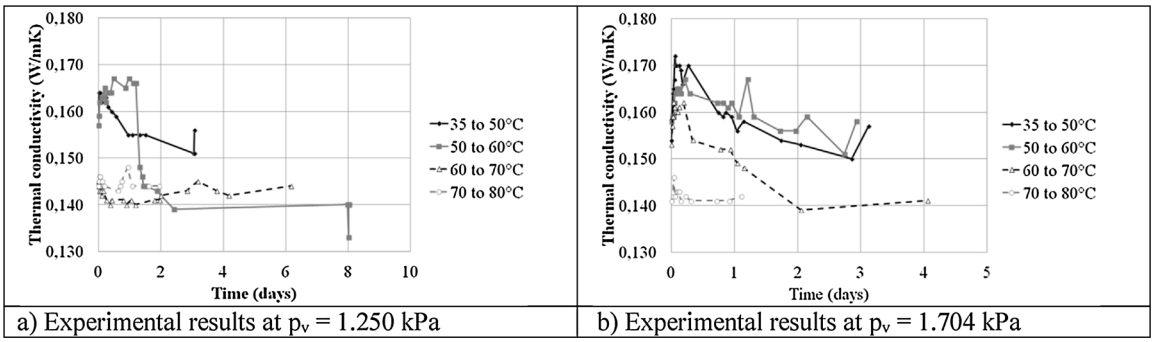

Fig. 8. Measured values of apparent thermal conductivity.

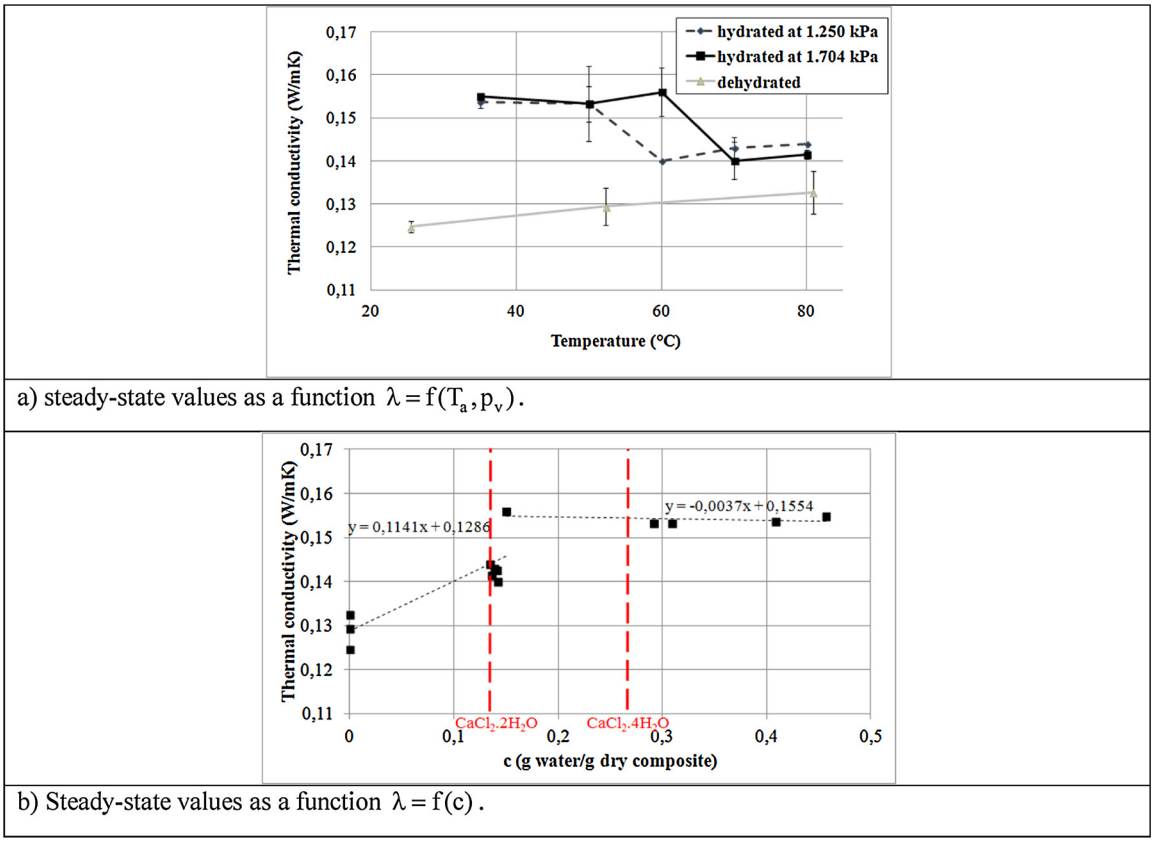

Fig. 9. Steady-state values of thermal conductivity.

Table 2
Thermal conductivities of silica and $CaCl_2$. Two first lines: estimated values of bed voidage based on bed density.

Medium	λ ($W\,m^{-1}\,K^{-1}$)	Remark	Ref.
$CaCl_2$ (s)	0.21	Bed with ~57% void	Karawacki [47]
$CaCl_2{\cdot}2H_2O$ (s)	0.19	Bed with ~60% void	Karawacki [47]
$CaCl_2$ (aq, sat.)	0.86		Karawacki [47]
$CaCl_2$ (s)	T = 30 °C: 1.33 40 °C ≤ T ≤ 100 °C: 1.49		Mirzaev [48]
$CaCl_2{\cdot}6H_2O$ (s/aq)	T = 20 °C: 1.49 T = 30 °C: 0.96 T ≥ 30 °C: λ = 0.0041*T* + 0.8	Solid at 20 °C Deliquescence at 30 °C followed by partial dehydration	Mirzaev [48]
$CaCl_2{\cdot}6H_2O$ (s/aq)	T = 38.7 °C: 0.540 (aq) T = 61.2 °C: 0.561 (aq) T = 23 °C: 1.09 (s)		Tatsidjodoung [54]
$CaCl_2{\cdot}6H_2O$ (s)	T = 10 °C: 0.61 T = 28 °C: 0.50		Nicolic [49]
$CaCl_2$ (aq)	30 °C ≤ T ≤ 60 °C: ~0.50	Slightly decreasing with T	Nicolic [49]
$CaCl_2$ (aq)	$\lambda = \lambda_{H_2O}(1 - 0.0020856f)$ 0.5969 at 10% salt, 300 K.	f: salt mass%. λ_{H_2O}($W.m^{-1}.K^{-1}$): 0.6096 at 27 °C; 0.6655 at 77 °C.	Akhmedova-Azizova [50]
SiO_2	T = 27 °C: 1.4 T = 127 °C: 1.5	Fused quartz	US Bureau of Standards [51]
$CaCl_2$ (s)	0.54	Bed with 23–35% void	Fopah-Lele [34]
$CaCl_2{\cdot}6H_2O$ (s)	0.7–0.93	Bed with 38–64% void	Fopah-Lele [34]
SiO_2	0.08	Effective, for dry silicagel "119", atmospheric pressure, porosity: 0.69	Björström [31]
SiO_2	~0.03, function of compression and contact resistance	Porosity: 95–97%	Afriyie [53]
SiO_2	0.016–0.055, function of pressure and density of the bed	Porosity: 96–98%	Karami [52]
SG62-$CaCl_2$	λ = 0.129 + 0.11c (c < 0.14 g/g) λ ≅ 0.155 (c > 0.14 g/g)		This work

from the literature are summarized in Table 2. The data from Karawacki et al. [47] cannot be fully used for the comparison with the present study, because they account relatively high bed voidage, but they confirm the trend of the negative influence of the bed voidage on the conductivity. The work of Mirzaev et al. [48] showed that the deliquescent salt is less conductive than the solid, anhydrous or hydrated salt. It seems hard to find distinct values for the various hydrates since there is some scattering in data between the studies, but Nicolic's work [49] confirmed that the solid hexahydrate is more conductive than the deliquescent salt. More systematic studies on $CaCl_2$ solutions,

like the work of Akhmedova-Azizova et al., suggested that the conductivity of concentrated $CaCl_2$ solution (20 wt.%) is $\sim 0.6\,W\,m^{-1}\,K^{-1}$ [50].

Regarding SG matrix, the intrinsic value of amorphous silica is given in Table 2 based on data from the US Bureau of Standards ([51,p. 99]), but it is indicative, since it refers to a bulk material. The SG matrix used in the present work has internal porosity ~72%, close to the silica gel "119" studied by Björström et al. [31], but less than the aerogels studied by Karami et al. [52] and Afriyie at al. [53].

Based on data in Table 2, the interpretation of values from Fig. 9b is the following one. At c = 0, corresponding to the dehydrated salt, the measured conductivity ($0.13\,W\,m^{-1}\,K^{-1}$ with slight influence of T as shown on Fig. 9a) is a joint value between pure silica, anhydrous salt and bed voidage (intra and interparticle) conductivities. The void fraction is higher in these conditions, since the salt is not swollen by water and corresponds to the value reported in [18], $0.38\,cm^3\,g^{-1}$.

At c ~ 0.14 g/g, $CaCl_2$ is in the dihydrate form and thus increases the occupation of the voids in the SG matrix. Although it is not clear how the intrinsic conductivity of the salt evolves, however the reduction of voids has a direct effect on the increase of the conductivity to $0.14\,W\,m^{-1}\,K^{-1}$.

For c > 0.14 g/g, the solid tetrahydrate form of $CaCl_2$ was not observed by XRD [18]. The salt further hydrates and becomes deliquescent in the pores, occupying even more volume in the SG porosity. In contrast, the thermal conductivity of the salt is known to decrease (as shown in Table 2), but this effect is counter-balanced by the voidage influence. This explains why the conductivity remains limited to $\sim 0.155\,W\,m^{-1}\,K^{-1}$.

In all the cases, thermal conductivity remains far below a simple combination of the conductivities of silica and salt. This suggests either too poor physical contact between the particles of the untapped bed or a high tortuosity of the thermal paths inside the particles.

3.4. Water migration

For the water migration experiment, the SG62L/$CaCl_2$ composite with bigger particle size (315–500 μm) was used, as explained in Section 2. Fig. 4 shows the column used for water migration measurements, with the definition of the initial conditions. The dehydrated material fraction had a residual water uptake of $c_1 = 0.011$ g/g, while the initial water uptake of the hydrated fraction was $c_2 = 0.435$ g/g (Fig. 4). Prior to the experiments, nitrogen circulated in the vessel, to avoid the undesired presence of moisture. The interface between the hydrated and dehydrated composites is located half of the distance between the 5th and the 6th aperture from the bottom, corresponding to the space coordinate x = 0.

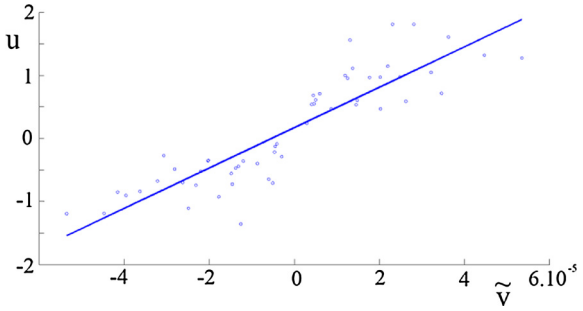

Fig. 11. $(u, \tilde{v})$ plot and mean square line.

The plot of water content as a function of position and time results in typical sigmoid curves (see Fig. 10). After 4 days, the water concentration significantly differs from its initial value at 5 cm from the interface. After 35 days, almost all the column is affected by moisture propagation. However, after 277 days, water concentration is still far away from its steady-state profile.

When the apparent diffusivity D depends on concentration c, it is convenient to use the Hall method. The method is suitable to extract D (c) from an experiment consisting in measuring the concentrations in a device where the diffusion is unidirectional [39,46]. By doing so, the medium is treated as pseudo-homogeneous and overall process is assumed to be limited by water migration, not by sorption phenomena.

According to the Hall's method, the diffusion coefficient D can be calculated by the following expression:

$$D(c) = \frac{1}{4h^2} + \frac{k\sqrt{\pi}}{2h^2}\exp(uh^2)\frac{c}{c_2}. \quad (1)$$

Where h is the slope and k is the offset, for the linear function

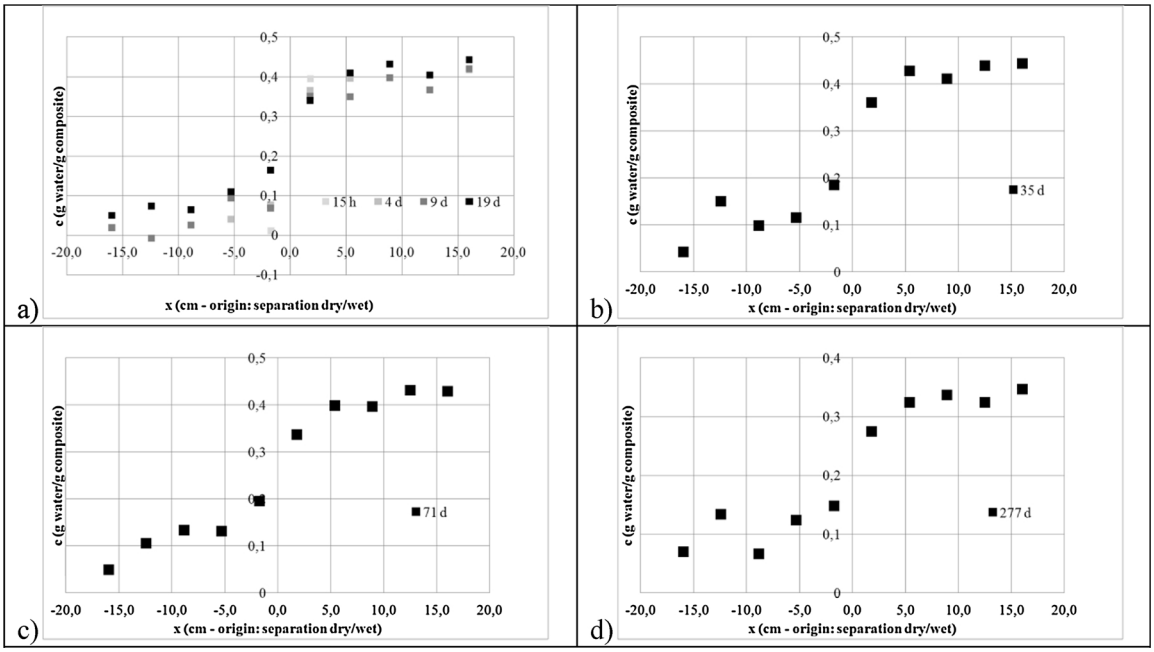

Fig. 10. Water concentration profiles at different times. Estimated uncertainty of water concentration is 2%. a) Until 19 days; b) After 35 days; c) After 71 days; d) After 277 days.

$u = hv + k$, calculated by the least squares method. The parameters u and v are calculated, using the reciprocal error function erf^{-1} for each c (x,t) measurement:

$$v = \frac{x}{\sqrt{t}} \tag{2}$$

$$u = \mathrm{erf}^{-1}\left(2\frac{c}{c_2} - 1\right) \tag{3}$$

All the experimental results from Fig. 10 were plotted on the u = u (v) graph (see Fig. 11), except those for which the measured value has no physical meaning. For the better understanding of this, (u, v) plots obtained from all the time values were studied separately (see Fig. A1 in Appendix A). A quite fair linear relationship can be obtained when considering instant water concentration snapshots (Fig. A1 in Appendix A). Furthermore, the slope becomes steeper with time progression. Similarly to a relaxation process, the observed trend is stronger at the beginning of the experiment, when $t \cong 0$, and attenuates with the time progression $t \to \infty$.

Applying the Hall's method as is would lead to the increase of D for concentration c and to the decrease of D with time t, but the original method assumes that D is a function of c only [39]. A modified Hall method was developed to interpret the results. The developed method is described by equations (Eqs. (A1)–(A7)) in Appendix A.

According to the developed method, the apparent diffusivity is given by the following relation:

$$\widetilde{D}(\Theta, c, t) = D(c)\Theta(t) = D(c)(1 + A\exp(-rt)) \tag{4}$$

Where A is the pre-exponential constant and r is the time constant.

Firstly, A and r were fitted on the modified Hall's plot based on experimental values (definition in appendix, graph in Fig. 11). The following values were obtained: $A = 40$ and $r = 3 \times 10^{-6}\,s^{-1}$. By doing this, the correlation coefficient of the modified Hall's plot is 0.8852. Secondly, the coefficients of the modified Hall's line are determined. The following values are obtained: $h = 3 \times 10^{4}$ and $k = 0.17$.

In (Eq. (4)), the diffusivity D(c) has the same form as in (Eq. (1)) of the original Hall's method. In order to use the modified Hall's method, developed in the present work, the determined coefficients h and k have to be introduced consequently to (Eq. (1)) and (Eq. (4)). However, a special attention must be paid to (Eq. (1)), when using coefficients h and k. Although it was suggested that D(c) increases with c, this trend is rather weak since the sign of k is rather uncertain (Fig. 11). On the contrary, there is a decrease of Θ by a factor of 40 between the initial and terminal experimental values that may be explained by a progressive modification of the structural properties of the composite in time. Therefore, the water migration inside the material slows down. The described trends are summarized in Fig. 12.

It is interesting to compare the obtained values with literature. The first benchmark is the Knudsen regime whose principal mechanism is based on the collisions between the diffusing gas species and the internal walls in solid pores. Knudsen Diffusivity is predicted by the following equation ([55,p. 136]):

$$D_{Knudsen}\left(\frac{cm^2}{s}\right) = 9700.R(cm).\sqrt{\frac{T(K)}{M(g/mol)}} \tag{5}$$

where M is the molar mass and R is the pore radius. In the present work, the pores radius has the distribution of ~5 nm by considering the dry material [18]. This yields in $\sim 2{\cdot}10^{-6}\,m^2\,s^{-1}$ of calculated Knudsen diffusivity, that is more than two orders of magnitude higher than the experimental diffusivity values.

The second benchmark is Aristov and coworkers work on a silicagel-$CaCl_2$ composite, with a value of $2 \times 10^{-7}\,m^2\,s^{-1}$. Aristov's experiments differed from the present paper in that (i) they did not exceed a few hours, (ii) they were performed with adsorption devices at a small scale, (iii) they used water vapor partial pressure as a control parameter and (iv) the salt content in the composite was lower, and (v) the porous structure of the silica gel was not the same [42].

According to Aristov, a possible explanation of the discrepancy with the Knudsen's diffusivity is the high tortuosity of the pores [42]. In the present work, the additional discrepancy may be due to the experimental differences (i and iv): the salt morphology inside the pores is modified with time, which progressively blocks water diffusion, possibly due to salt rearrangement.

In order to compare the rates of heat and mass transfers, one can compare the values of D or $\widetilde{D}$ and thermal diffusivity. Based on a measured packing density of $700\,kg\,m^{-3}$ and an assumed specific heat of $600\,J\,kg^{-1}\,K^{-1}$ (based on specific heats of $CaCl_2{\cdot}2H_2O$ and silica), thermal diffusivity is equal to: $D_{thermal} \cong 3.5 \times 10^{-7}\,m^2\,s^{-1}$, which means that heat transfer is at least one order of magnitude higher than mass transfer.

From the practical point of view, the extraction of produced heat is fast compared to the migration of water towards the reacting sites. This means that the heat restitution by water sorption should be made either by a design that reduces the path taken by water or by imposing to the reactants a relative movement. This justifies using a blower for moist air, or a vibro-fluidizer as proposed in the frame of SoTherCo research project (http://www.sotherco.eu/en/index_en.html).

In contrast, water diffusion is still sufficient to propagate contamination by water in a storage tank of dehydrated composite. A stratified storage system, where reacted and unreacted composite are stored together in the same tank, is therefore not appropriate even at the scale of several cubic meters. Water propagation at the smallest times in the experiments however shows that water exchange is still significant and spoils the dehydrated material.

4. Conclusions

Heat and mass transfer properties were measured for a newly synthesized SG/$CaCl_2$ 40–43 wt.% composite, as a function of adsorbed water concentration.

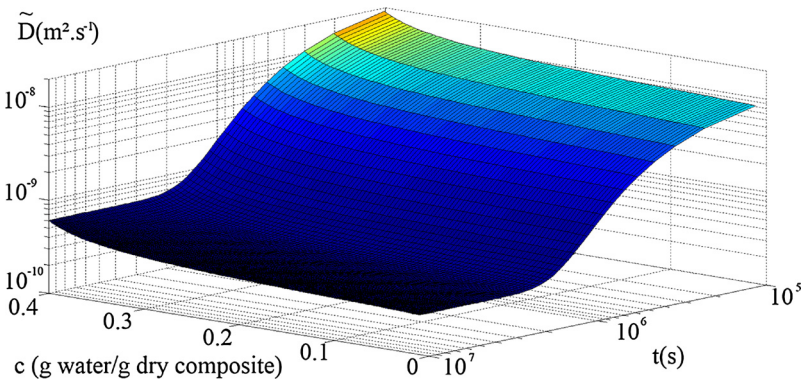

Fig. 12. Dependence of apparent $\widetilde{D}$ values on time and concentration, for different experiment durations.

The apparent thermal conductivity was measured successfully in a controlled atmosphere. In equilibrium conditions, it is comprised between 0.129 and 0.155 $W\,m^{-1}\,K^{-1}$. This value depends on the intrinsic conductivity of the silica gel but is modified by the presence of calcium chloride and of the void fraction. The salt is subjected to phase changes, from the anhydrous form to a deliquescent solution, with a modification of the pathways available for heat transport. Despite drastic modifications of the salt crystallinity, the observed variations are limited, due to the antagonist influence of the reduction of the void fraction and the smaller conductivity of the salt solution.

For water apparent diffusivity, a larger scale sample was necessary. Chemical and structural characterizations showed no significant difference, especially on the intra-particle homogeneity, with respect to the laboratory scale sample, which is in itself of industrial interest. The measurement of diffusivity was based on a diffusion column and on the measurement of diffusion profiles. The Hall method was modified, in order to highlight variations with water content. It was first assumed that the apparent diffusivity depends on concentration c, but not on time t, which proved incorrect. To solve this, a function was introduced in the Fick's equation, and a change of variable was made, to adapt the Hall method.

The method used to study the influence of moisture on diffusivity is less sensitive than the method used for conductivity. The observed variation, supposed to be small, is not significant, despite, again, the presence of different forms of $CaCl_2$. However, the diffusivity is divided by ~40 during the present long term experiment, due to the salt rearrangement inside the silica gel pores. It is believed that the tortuosity of the pathways available for the water migration is increased.

Acknowledgement

The authors acknowledge the European Commission for a FP7 funding (SoTherCo collaborative project, grant agreement nr. 295775).

Appendix A

Fig. A1 shows a first attempt to apply Hall's method. The slopes of the regressions lines do not coincide at the shortest and longest time values.

Since this data treatment is not compatible with the original Hall method, a modified method is proposed. It is assumed that apparent diffusivity is also a function of time, i.e. $\widetilde{D} = \widetilde{D}(c, t)$. Changes of the apparent value may be explained by changes in the salt morphology inside pores. This is plausible, since calcium chloride is subject to crystalline changes. In literature, it is often referred to tortuosity that is introduced to divide the diffusivity in the Fick equation [55]. It is thus assumed that $\widetilde{D}$ can be separated in two functions: D that accounts for the intrinsic diffusion phenomena and Θ that accounts for the changes of tortuosity with time:

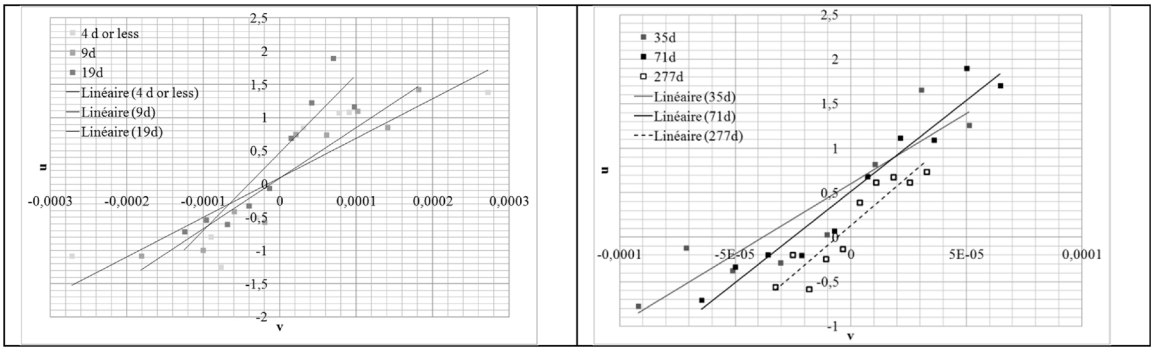

Fig. A1. (u, v) plot and mean square lines, for different time values, based on classical Hall method.

$$\widetilde{D}(\Theta, c, t) = D(c)\Theta(t) \tag{A1}$$

The Fick's equation writes:

$$\frac{1}{\Theta(t)}\frac{\partial c}{\partial t} = D(c)\frac{\partial^2 c}{\partial x^2} \tag{A2}$$

A modified time variable $\tilde{t} = \tilde{t}(\Theta, t)$ is introduced, leading to:

$$\frac{\partial}{\partial t}\tilde{t}(\Theta, t) = \frac{\partial}{\partial \Theta}\tilde{t}(\Theta, t)\frac{d}{dt}\Theta(t), \tag{A3}$$

Assuming that $\frac{\partial}{\partial t}\tilde{t}(\Theta, t) = \Theta(t)$, one gets:

$$\tilde{t}(\Theta, t) = \int \Theta(t)dt, \tag{A4}$$

leading to a modified form of the Fick's equation:

$$\frac{\partial c}{\partial \tilde{t}} = D(c)\frac{\partial^2 c}{\partial x^2}. \tag{A5}$$

Eq. (A5) is now identical to the Fick's law with concentration dependent diffusivity, making it possible to reuse the Hall method with:

$$\tilde{v} = \frac{x}{\sqrt{\tilde{t}}}, \tag{A6}$$

Eqs. (2) and (3) still hold true and D(c) is calculated using a $(u, \tilde{v})$ modified Hall's plot. The apparent diffusivity is calculated using Eq. (1).

For $\Theta(t)$, the following form is proposed in present experiments:

$$\Theta(t) = 1 + A\exp(-rt). \quad (A7)$$

The initial value of $\widetilde{D}$ is thus $D(c)(1 + A)$ and it tends to $D(c)$ for long times. The curve fitting is made as follows. First, the $(u, \tilde{v})$ plot is drawn for different values of r and A. In order to match as much as possible the linearity, the highest linear correlation coefficient is seeked. Second, h and k coefficients are determined using the least square method.

References

[1] J.A. Quinnell, J.H. Davidson, Mass transfer during sensible charging of a hybrid absorption/sensible storage tank, Energy Procedia 30 (2012) 353–361.
[2] J.A. Quinnell, J.H. Davidson, Heat and mass transfer during heating of a hybrid absorption/sensible storage tank, Sol. Energy 104 (2014) 19–28.
[3] H. Lahmidi, S. Mauran, V. Goetz, Definition, test and simulation of a thermochemical storage process adapted to solar thermal systems, Sol. Energy 80 (2006) 883–893.
[4] S. Mauran, H. Lahmidi, V. Goetz, Solar heating and cooling by a thermochemical process. First experiments of a prototype storing 60 kW h by a solid/gas reaction, Sol. Energy 82 (2008) 623–636.
[5] B. Michel, N. Mazet, S. Mauran, D. Stitou, J. Xu, Thermochemical process for seasonal storage of solar energy: characterization and modeling of a high density reactive bed, Energy (Oxford, United Kingdom) 47 (2012) 553–563.
[6] V.M. van Essen, H.A. Zondag, J. Cot Gores, L.P.J. Bleijendaal, M. Bakker, R. Schuitema, W.G.J. van Helden, Z. He, C.C.M. Rindt, Characterization of $MgSO_4$ hydrate for thermochemical seasonal heat storage, J. Solar Energy Eng. 131 (2009) 0410141–0410147.
[7] M. Molenda, J. Stengler, M. Linder, A. Wörner, Reversible hydration behavior of $CaCl_2$ at high H_2O partial pressures for thermochemical energy storage, Thermochim. Acta 560 (2013) 76–81.
[8] A. Frazzica, A. Freni, Adsorbent working pairs for solar thermal energy storage in buildings, Renew. Energy 110 (2017) 87–94.
[9] A. Grekova, L. Gordeeva, Y. Aristov, Composite sorbents 'Li/Ca halogenides inside multi-wall carbon nano-tubes' for thermal energy storage, Sol. Energy Mater. Sol. Cells 155 (2016) 176–183.
[10] B. Michel, N. Mazet, S. Mauran, D. Stitou, J. Xu, Thermochemical process for seasonal storage of solar energy: characterization and modeling of a high density reactive bed, Energy 47 (2012) 553–563.
[11] Y. Zhao, R. Wang, Y. Wang, N. Yu, Development of $SrBr_2$ composite sorbents for a sorption thermal energy storage system to store low-temperature heat, Energy 115 (2016) 129–139.
[12] A. Solé, X. Fontanet, C. Barreneche, I. Martorell, A. Fernandez, L.F. Cabeza, Parameters to take into account when developing a new thermochemical energy storage system, Energy Procedia 30 (2012) 380–387.
[13] J. Jaenchen, D. Ackermann, H. Stach, W. Broesicke, Studies of the water adsorption on zeolites and modified mesoporous materials for seasonal storage of solar heat, Sol. Energy 76 (2004) 339–344.
[14] H. Stach, J. Mugele, J. Jaenchen, E. Weiler, Influence of cycle temperatures on the thermochemical heat storage densities in the systems water/microporous and water/mesoporous adsorbents, Adsorption 11 (2005) 393–404.
[15] A. Permyakova, S. Wang, E. Courbon, F. Nouar, N. Heymans, P. D'Ans, N. Barrier, P. Billemont, G.D. Weireld, N. Steunou, M. Frère, C. Serre, Design of salt-metal organic framework composites for seasonal heat storage applications, J. Mater. Chem. A 5 (2017) 12889–12898.
[16] R. Olives, S. Mauran, A highly conductive porous medium for solid-gas reactions: effect of the dispersed phase on the thermal tortuosity, Transp. Porous Media 43 (2001) 377–394.
[17] Y. Aristov, M. Tokarev, G. Cacciola, G. Restuccia, Selective water sorbents for multiple applications, 1. $CaCl_2$ confined in mesopores of silica gel: sorption properties, React. Kinet. Catal. Lett. 59 (1996) 325–333.
[18] E. Courbon, P. D'Ans, A. Permyakova, O. Skrylnyk, N. Steunou, M. Degrez, M. Frère, Further improvement of the synthesis of silica gel and $CaCl_2$ composites: enhancement of energy storage density and stability over cycles for solar heat storage coupled with space heating applications, Sol. Energy 157 (2017) 532–541.
[19] A. Grekova, L. Gordeeva, Y. Aristov, Composite 'LiCl/vermiculite' as advanced water sorbent for thermal energy storage, Appl. Therm. Eng. 124 (2017) 1401–1408.
[20] A. Grekova, L. Gordeeva, Z. Lu, R. Wang, Y. Aristov, Composite 'LiCl/MWCNT' as advanced water sorbent for thermal energy storage: sorption dynamics, Sol. Energy Mater. Sol. Cells 176 (2018) 273–279.
[21] H. Demir, M. Mobeli, S. Ülkü, The use of metal piece additives to enhance heat transfer rate through an unconsolidated adsorbent bed, Int. J. Refrig. 33 (2010) 714–720.
[22] G. Balasubramanian, M. Ghommem, M. Hajj, W. Wong, J. Tomlin, I. Puri, Modeling of thermochemical energy storage by salt hydrates, Int. J. Heat Mass Transf. 53 (2010) 5700–5706.
[23] K. N'Tsoukpoe, G. Restuccia, T. Schmidt, X. Py, The size of sorbents in low pressure sorption or thermochemical energy storage processes, Energy 77 (2014) 983–998.
[24] I. Simonova, A. Freni, G. Restuccia, Y. Aristov, Water sorption on composite "silica modified by calcium nitrate, Microporous Mesoporous Mater. 122 (2009) 223–228.
[25] M. Ghommem, G. Balasubramanian, M.R. Hajj, W.P. Wong, J.A. Tomlin, I.K. Puri, Release of stored thermochemical energy from dehydrated salts, Int. J. Heat Mass Transf. 54 (2011) 4856–4863.
[26] B. Mette, H. Kerskes, H. Drück, Experimental and numerical investigations of different reactor concepts for thermochemical energy storage, Energy Procedia 57 (2014) 2380–2389.
[27] A. Fopah Lele, F. Kuznik, H. Rammelberg, T. Schmidt, W. Ruck, Thermal decomposition kinetic of salt hydrates for heat storage systems, Appl. Energy 154 (2015) 447–458.
[28] M. Gaeini, H. Zondag, C. Rindt, Effect of kinetics on the thermal performance of a sorption heat storage reactor, Appl. Therm. Eng. 102 (2016) 520–531.
[29] K. Ndiaye, S. Ginestet, M. Cyr, Modelling and experimental study of low temperature energy storage reactor using cementitious material, Appl. Therm. Eng. 110 (2017) 601–615.
[30] V. Valkov, Measurement technique for determination of the thermophysical properties of thermochemical storage materials, Proc. World Conf., 3rd, Exp. Heat Transfer, Fluid Mech. Thermodyn. (1993) 529–536.
[31] H. Bjurström, E. Karawacki, B. Carlsson, Thermal conductivity of a microporous particulate medium: moist silica gel, Int. J. Heat Mass Transf. 27 (1984) 2025–2036.
[32] Y. Tanashev, Y. Aristov, Thermal conductivity of a silica gel + calcium chloride system: the effect of adsorbed water, J. Eng. Phys. Thermophys. 73 (2000) 876–883.
[33] H. Freni, M.M. Tokarev, G. Restuccia, A.G. Okunev, Y. Aristov, Thermal conductivity of selective water sorbents under the working conditions of a sorption chiller, Appl. Therm. Eng. 22 (2002) 1631–1642.
[34] A. Fopah Lele, K. N'Tsoukpoe, T. Osterland, F. Kuznik, W. Ruck, Thermal conductivity measurement of thermochemical storage materials, Appl. Therm. Eng. 89 (2015) 916–926.
[35] D. Lager, Thermal analysis on organic phase change materials for heat storage applications, AIP Conference Proceedings, Terchova (SK), 2016.
[36] Y. Tanashev, A. Krainov, Y. Aristov, Thermal conductivity of composite sorbents 'salt in porous matrix' for heat storage and transformation, Appl. Therm. Eng. 61 (2013) 401–407.
[37] M. Kandula, On the effective thermal conductivity of porous packed beds with uniform spherical particles, J. Porous Media 14 (2011) 919–926.
[38] M. Winterberg, E. Tsotsas, Correlations for e!ective heat transport coe$cients in beds packed with cylindrical particles, Chem. Eng. Sci. 55 (2000) 5937–5943.
[39] L. Hall, An analytical method of calculating variable diffusion coefficients, J. Chem. Phys. 21 (1953) 87–89.
[40] J. Delgado, A critical review of dispersion in packed beds, Heat Mass Transf. 42 (2006) 279–310.
[41] E. Courbon, M. Frère, N. Heymans, P. D'Ans, Hygroscopic composite material, Patent no. 2015/197788 A1.
[42] Y. Aristov, I. Glaznev, A. Freni, G. Restuccia, Kinetics of water sorption on SWS-1L (calcium chloride confined to mesoporous silica gel): influence of grain size and temperature, Chem. Eng. Sci. 61 (2006) 1453–1458.
[43] U. Hammerschmidt, V. Maier, New transient hot-bridge sensor to measure thermal conductivity, thermal diffusivity, and volumetric specific heat, Int. J. Thermophys. 27 (2006) 840–856.
[44] R. Model, R. Stosch, U. Hammerschmidt, Virtual experiment design for the transient hot-Bridge sensor, Int. J. Thermophys. 28 (2007) 1447–1460.
[45] U. Hammerschmidt, W. Sabuga, Transient hot wire (THW) method: uncertainty assessment, Int. J. Thermophys. 21 (2000) 1255–1278.
[46] J. Crank, The Mathematics of Diffusion, 2nd ed., Clarendon Press, Oxford, 1975.
[47] E. Karawacki, A. Lundén, Thermal transport studies by transient hot strip method of salts used in heat storage devices, High Temp.—High Press. 21 (1989) 183–187.
[48] S. Mirzaev, Y. Yakubov, A. Akhmedov, S. Boltaev, O. Shodiev, Experimental study of the temperature dependence of the $CaCl_2$, $SrCl_2$, $CaCl_2.6H_2O$, and $SrCl_2.6H_2O$ absorbent heat conductivity, Appl. Sol. Energy 32 (1996) 65–70.
[49] R. Nicolic, J. Tripkovic, Measurements of thermal conductivities of some low-melting materials in a concentric cylinder apparatus, Appl. Phys. A 44 (1987) 293–297.
[50] L. Akhmedova-Azizova, I. Abdulagatov, Thermal conductivity of aqueous $CaCl_2$ solutions at high temperatures and high pressures, J. Solut. Chem. 43 (2014) 421–444.
[51] US Department of Commerce and National bureau of Standards. Thermal conductivity of selected materials (1996).
[52] P. Karami, E. Afriyie, P. Norberg, K. Gudmundsson, A study of the thermal conductivity of granular silica materials for VIPs at different levels of gaseous pressure and external loads, Energy Build. 85 (2014) 199–211.
[53] E. Afriyie, Textural and thermal conductivity properties of a low density mesoporous silica material, Energy Build. 75 (2014) 210–215.
[54] P. Tatsidjodoung, N.L. Pierrès, L. Luo, A review of potential materials for thermal energy storage in building applications, Renew. Sustain. Energy Rev. 18 (2013) 327–349.
[55] D. Ruthven, Principles of Adsorption and Adsorption Processes, John Wiley & Sons, 1984.